DOI: 10.1002/ ((please add manuscript number))
Article type: Full Paper

Intraband Cooling in All-Inorganic and Hybrid Organic-Inorganic Perovskite Nanocrystals

*Benjamin T. Diroll and Richard D. Schaller**

Dr. B. T. Diroll and Prof. Dr. R. D. Schaller
Center for Nanoscale Materials, Argonne National Laboratory, Lemont, IL 60439
E-mail: schaller@anl.gov
R. D. Schaller
Department of Chemistry, Northwestern University, Evanston, IL 60208

Keywords: perovskites, nanocrystals, intraband, hot carriers

Abstract: Intraband relaxation in all-inorganic cesium lead tribromide ($CsPbBr_3$) and hybrid organic-inorganic formamidinium lead tribromide ($FAPbBr_3$) nanocrystals is compared experimentally using ultrafast spectroscopy. Carrier cooling is reported for both compositions of nanocrystals over a similar range of particle sizes for different excitation energies, sample temperatures, and excitation fluences. Hot carriers in $CsPbBr_3$ nanocrystal samples consistently exhibit slower cooling than $FAPbBr_3$ nanocrystal samples in the single electron-hole pair *per* nanocrystal regime. In both compositions, long-lived hot carriers (>2 ps) are only observed at excitation densities corresponding to generation of multiple electron-hole pairs *per* nanocrystal—and concomitant Auger recombination. This evidence of prolonged hot carriers only under conditions of multiple electron-hole pairs *per* nanocrystal, driven by the Auger process, is distinct from previous reports in bulk hybrid perovskite materials of persistent hot carriers at low excitation fluences. Time-resolved photoluminescence confirms the rapid cooling of carriers in the low-fluence (single electron-hole pair *per* nanocrystal) regime. Intraband relaxation processes, as a function of excitation energy, size, and temperature are broadly consistent with other nanocrystalline semiconductor materials.

1. Introduction

The emergence of hybrid organic-inorganic plumbotrihalide perovskite materials with organic cations (methylammonium, MA, or formamidinium, FA) as optoelectronic materials of high quality[1,2] has focused research on unique properties that are reported to emerge from the presence of organic cations *versus* other potential origins. For example, it has been long known that the free rotation of organic cations in hybrid perovskites leads to a much larger dielectric values at low frequencies.[3,4] In addition to claimed effects on the exciton binding energy,[5–7] carrier lifetime,[6,8,9] and Auger recombination,[10] the choice of cation has been implicated in determining the rate of carrier cooling.[11,12] A prominent initial report indicated that hybrid perovskites support long-lived hot carriers at low excitation fluences, whereas all-inorganic systems do not.[12] This was attributed to charge screening from the plastic crystal nature of the organic cations.[12,13] The presence of persistent energetic carriers due to slow intraband relaxation would mark out hybrid perovskites as promising materials to beat the Shockley-Queisser limit in hot carrier photovoltaics.[14,15] But the influence of cations on carrier cooling in plumbotrihalide perovskites remains contested. Initial accounts have been supported—for example by reported slow intraband cooling in $FAPbI_3$ nanocrystals[16]—but also contradicted. On one hand, other experiments on cooling relate slow intraband cooling in bulk all-inorganic $CsPbX_3$[11,17] (above threshold fluences) or persistent hot carrier emission in bulk hybrid tin trihalide perovskites at low temperatures, for which the organic molecules have reduced rotational freedom.[18] Other reports claim that cooling in both hybrid and all-inorganic systems are comparable to other semiconductors, with sub-picosecond cooling times.[11,19,20]

Here we present a study of intraband cooling in nanocrystalline perovskites of the compositions $FAPbBr_3$ and $CsPbBr_3$ synthesized by hot injection[21,22] as functions of size, temperature, excitation photon energy, and excitation fluence. These measurements disambiguate the role of several possible variables and provide a unifying picture in which intraband cooling of all-inorganic perovskite nanocrystals is actually somewhat slower than

hybrid perovskite nanocrystals in the low-excitation (less than one electron-hole pair *per* nanocrystal) regime. This is consistent across all measured sizes, excitation energies, and temperatures as well as in-line with theoretical predictions based upon the density of low-energy phonon states (of the bulk material).[11,20] Persistent hot carriers are only found under high-intensity excitation conditions, greater than in the limit of one electron-hole pair *per* nanocrystal, which is well-understood under the framework provided by past studies of Si or GaAs[23–28] and other semiconductor nanocrystals.[29–31]

2. Intraband Cooling at Low Excitation Fluence in $CsPbBr_3$ and $FAPbBr_3$ Nanocrystals

2.1. Size-Dependence of Intraband Cooling

Figure 1 contains typical transient absorption data of $CsPbBr_3$ and $FAPbBr_3$ nanocrystals in solution collected with an average number of electron-hole pairs *per* nanocrystal of less than one (here $\langle n \rangle < 0.2$), here exciting with 3.1 eV photons. Crystal structures of these materials appear consistent with literature reports—orthorhombic for $CsPbBr_3$[32] and cubic for $FAPbBr_3$.[22] Both compositions show the formation of a bleach corresponding to the excitonic absorption of the samples. Establishing a quasi-thermal energy distribution of photoexcited carriers is reported to take less than 100 fs in bulk $MAPbI_3$[33] and 300 fs in bulk $CsPbI_3$.[17] Here, non-thermal distributions of carriers, evidenced by changes in the shape of the $\Delta\alpha$ spectrum at higher probe energies relative to the excitonic bleach, suggest thermal distributions, in which carriers in equilibrium with each other (but not with the lattice), are established in approximately 150 fs in both $CsPbBr_3$ and $FAPbBr_3$ nanocrystals at 295 K. After establishing a quasi-thermal distribution, carrier temperature may be estimated by fitting the asymmetric bleaching feature with a Boltzmann thermal distribution of the form

$$\Delta\alpha = ae^{\left(-\frac{E}{kT}\right)} + b$$

where k is Boltzmann's constant, E is photon energy, a is a scalar (negative where $\Delta\alpha < 0$), and b is an offset taking into account photoinduced absorptionon the higher-energy side of the

bleach feature.[12,34,35] Qualitatively, regions of the spectral map that appear diagonal in Figure 1a and 1b, which here last for *ca.* 1 ps, indicate continued carrier cooling to the band-edge. As with most other reports of intraband relaxation in nanocrystals,[36] predicted slowing of carrier cooling[37–39]—even in weak confinement—is absent. (The Bohr radius of $CsPbBr_3$ has been estimated as 7 nm[21] and the Bohr radius of $FAPbBr_3$ has been estimated as 3.5 nm.[40]) This is true even though symmetric carrier masses should prevent electron-hole energy transfer processes.[41] The normalized spectral line-cuts in Figures 1c and 1d further confirm that the high-energy spectral tail indicative of hot carriers is absent by 2 ps delay time. Under this circumstance, the bleach formation time, which represents filling of the band-edge excitonic state, represents a good indication of intraband cooling times.

Excitonic bleach kinetics for a series of nanocrystals ($\langle n \rangle < 0.2$) of varying sizes are shown in Figures 1e and 1f, with solid lines representing exponential fits to the data in open circles. Earlier reports of semiconductor nanocrystal intraband relaxation show that the lifetime increases with particle size.[42,43] Such a trend is apparent in Figure 1g for $CsPbBr_3$, but not for $FAPbBr_3$ nanocrsytals over a similar size range. Reports for intraband relaxation in $MAPbBr_3$ nanocrystals also show this anomalous size-dependence.[44] Even for $CsPbBr_3$ nanocrystals, the size-dependence of intraband relaxation times is weaker than is observed for other nanocrystal compositions. One conceivable reason is that the plumbotrihalide perovskites studied here may be less susceptible to coupling of low-frequency Pb-Br derived phonons with organic ligand vibrational states on the nanocrystal surface, although experimental measurements of the low-energy density of states are similar in $CsPbBr_3$ to other nanocrystals.[45–50] These surface phonons may still explain deviation of nanocrystals and bulk materials in intraband cooling behavior. Another potential origin is that in most quantum-confined materials, the excess energy of an electronic pump, which can also have a substantial influence on intraband relaxation (described immediately below), is less readily decoupled from the particle size and often not decoupled at all, with all measurements collected at the same excitation wavelength.

Here, the size and excess energy are weakly coupled in the case of $FAPbBr_3$ and almost totally decoupled for $CsPbBr_3$.

2.2. Dependence of Intraband Cooling on the Pump Energy and Sample Temperature

Pump photon energy in excess of the semiconductor band gap (or the monitored feature[43,51]) is well-understood to generate an initial population of carriers at higher quasi-temperature which results in a longer total cooling time.[34,52] Data consistent with this effect is observed under low fluence conditions ($\langle n \rangle < 0.2$) for both $CsPbBr_3$ and $FAPbBr_3$, as shown in **Figure 2**. The fastest relaxation, essentially instrument-response limited, for the samples was observed with 2.58 eV excitation, closest to the room temperature band-gaps, estimated from the excitonic bleach at 2.50 eV for $CsPbBr_3$ and 2.39 eV for $FAPbBr_3$ for these particular samples. For more energetic pump photon energies, shown in Figures 2c and 2d, the intraband relaxation time increases substantially. $CsPbBr_3$ displays both slower cooling for a given excess photon energy and greater sensitivity of changes in the pump energy compared to $FAPbBr_3$. As described above and shown in Figures 2e and 2f, the origin of the apparent increase in the cooling time is the higher initial temperature of hot electrons that leads to a longer relaxation, which remains less than 2 ps for all measurements with $\langle n \rangle < 0.2$.

Figures 3a and 3b show the temperature-dependent intraband cooling dynamics of the samples performed on solid nanocrystal films, which facilitate measurements made in a vacuum cryostat. Intraband cooling is not expected to be strongly affected by a solid *versus* solution sample (differences measured in this case are very small), although outcoupling of heat from the lattice (which itself has very low thermal conductivity[53]) to the surroundings will change from a solution environment to a vacuum environment. Unlike bulk materials (particularly $CsPbBr_3$[54]), the probed nano-sized samples exhibit no clear evidence of a phase transition evidenced by a non-monotonic change in band gap.[55–59] Transient absorption data taken at low fluence ($\langle n \rangle \approx 0.1$) at the excitonic bleach maximum in Figures 2c and 2d show the slowing of intraband cooling with reduced temperatures, which occurs in both $CsPbBr_3$ and $FAPbBr_3$

nanocrystals. The change is more dramatic for $FAPbBr_3$, but for all measured temperatures, relaxation time was slower for $CsPbBr_3$ than $FAPbBr_3$. The changes in intraband cooling times of the perovskite nanocrystals fall between CdSe nanocrystals (which do not change noticeably) and PbSe nanocrystals, which show a substantial increase in intraband cooling times for temperatures below 200 K.[51] In past work, this change in the rate of intraband cooling with temperature has been taken as an indication of the possibility that multiphonon processes help to break the theoretical phonon bottleneck in quantum confined systems, a mechanism which appears operative in this case as well.[45,51]

Importantly, in no experiments at low fluence, whether as a function of nanocrystal size, pump energy, or temperature, exhibit measureable populations of hot carriers lasting longer than a few picoseconds in either all-inorganic or hybrid perovskite nanoparticles. For all measurements described to this point, under similar conditions, $CsPbBr_3$ nanocrystals actually show somewhat longer intraband relaxation times than $FAPbBr_3$ nanocrystals. These results contradict to at least two reports comparing bulk-like microstructures of $MAPbBr_3$ and $CsPbBr_3$[12,13] and a detailed study of $FAPbI_3$ nanocrystals.[16] In those works, persistent hot carriers lasting hundreds of picoseconds are reported to derive from screening by the well-understood plastic crystal nature of hybrid plumbotrihalide perovskites.[3] Instead, our work is more consistent with other findings on bulk and nanocrystalline $MAPbX_3$,[18,34,44,60] showing comparatively rapid intraband relaxation at low fluence, and theoretical predictions that the larger density of states at low energies in hybrid perovskites yields faster carrier cooling.[11] Indeed, intraband relaxation measurements using two-pump excitations (interband excitation followed by intraband excitation) have also shown that cooling is faster in $FAPbBr_3$ than $CsPbBr_3$ and in both cases remains sub-picosecond up to carrier densities as high as 2×10^{18} cm^{-3}.[20] For reference, 1 electron-hole pair *per* nanocrystal in a 10 nm cube represents 2×10^{18} cm^{-3}, although the comparison is not perfect due to the absence of carrier diffusion between particles (here in solution).

3. Intraband Cooling at High Excitation Fluence

With this foundation, measurements were performed as a function of excitation intensity. Two-dimensional transient absorption data at high fluence for typical samples of $CsPbBr_3$ and $FAPbBr_3$ nanocrystals are shown in **Figures 4a and 4b**, respectively. Under conditions with multiple electron-hole pairs *per* nanocrystal, persistent hot carriers are evident in the data to at least 100 ps delay times, which is notably two orders of magnitude longer than under low fluence conditions. In contrast to Figures 1c and 1d, Figures 4c and 4d show a blue tail of the photoinduced bleach feature persist for hundreds of picoseconds. Direct comparison of the exciton bleaching dynamics as a function of fluence shown in Figures 4e and 4f can undersell differences in carrier cooling which occur in the multiple electron-hole pairs *per* nanocrystal regime because it does not account for changes in the band-width of the bleaching feature. For example, clear regions of carrier cooling are apparent in the two-dimensional maps or line-cuts in Figures 4a-4d out to time delays of ~100 ps, but fitting of data at the excitonic peak in Figures 4e and 4f suggests an increase in lifetime of only ~30 percent for both $CsPbBr_3$ and $FAPbBr_3$ compared to the intraband cooling times at low fluence, albeit with a clear threshold in the multiexciton regime. (See Figure S5)

To provide a better picture of carrier temperature with time, the blue tail of transient absorption data was fitted with a Boltzmann distribution for several fluences to estimate the temperature of carriers with time, as described above and in the experimental details in accordance with previous literature.[17,34] As noted above, at low fluences, carriers cool exponentially on a sub-picosecond time-scale from initial carrier temperatures of ~1000 K for $CsPbBr_3$ and ~1200 K for $FAPbBr_3$, essentially the same result from fitting the excitonic bleach feature in TA directly, as noted above. Initial cooling rates determined from the derivative of the carrier temperature estimates are ~0.3 eV/ps for $CsPbBr_3$ and ~0.5 eV/ps for $FAPbBr_3$, at both high and low fluence. At higher fluences, which generate higher initial temperatures and

more than one exciton *per* nanocrystal, hot carriers persist for much longer due to Auger-recombination-derived heating.[28,29,61] Carrier temperatures in this regime decay in a bi- or even tri-exponential manner similar to earlier reports,[16] with the longer time-scale reasonably close to the estimated Auger recombination times. (See Figure S6 and Tables S1 and S2) The somewhat longer hot carrier bleaching observed under Auger recombination conditions for the $FAPbBr_3$ reflect longer Auger recombination times in the hybrid perovskite, which are shown estimated for biexcitonic Auger recombination in Figure S6 from fluence-dependent TA data and previously attributed to differences in the Coulombic interaction.[10]

One of the largest possible contributions to the variety of literature findings on carrier cooling rates in perovskites arises from differing excitation densities in measurements. In most power-dependent studies, slow cooling occurs only above threshold fluences.[17,34,52,62,63] which may be related to persistent heating due to Auger recombination occurring with higher excitation densities.[52] In nanocrystals, distinct from bulk materials, this applies when the number of electron-hole pairs *per* nanocrystal is greater than one, due to quantization of relaxation effects.[64] But Auger-derived slow cooling is hardly unique to hybrid perovskites: it occurs in virtually all semiconductor materials.[25,27,29,31,35,44,65,66]

4. Photoluminescence of Hot Carriers

Time-resolved photoluminescence experiments presented in **Figure 5** confirm that persistent hot carrier emission occurs at high excitation fluences, but not at low fluences, in these perovskite nanoparticles. Figures 5a and 5b show two-dimensional maps of $CsPbBr_3$ and $FAPbBr_3$, respectively, at an average of less than one exciton *per* nanocrystal followed in Figures 5c and 5d by photoluminescence maps with many excitons *per* nanocrystal. As in transient absorption maps, the data at high fluence show a broadening of the emission band at early time. Line plots comparing the first 50 ps of emission from low-fluence and high-fluence regimes to the time-integrated emission, confirm that substantial hot carrier emission is only

observed at high fluence. In photoluminescence, the broadening is both to the red, most likely from biexicton emission,[67] and blue, arising from the thermal distribution of hot carriers. These photoluminescence measurements display no evidence of a uniquely slow carrier cooling behavior in either all-inorganic or hybrid organic-inorganic plumbotribromide perovskites.

5. Conclusion

Intraband relaxation of all-inorganic and hybrid organic-inorganic nanocrystals of similar band-gap and structure has been examined as a function of the nanocrystal size, excitation wavelength, sample temperature, and excitation density. These experiments suggest that in contrast to some literature reports for bulk materials and some nanocrystals, carrier cooling in hybrid organic-inorganic perovskite nanocrystals such as $FAPbBr_3$ is unremarkable—occurring on a sub-picosecond time-scale at low excitation densities. In fact, experimental measurements consistently show that in all-inorganic perovskite nanocrystal materials actually show somewhat longer intraband relaxation under low fluence conditions for all sizes, temperatures, and excitation energies used, as in fact predicted for the bulk materials theoretically.[11] Only under conditions in which multiple excitons are generated *per* nanocrystal does the process of speed of carrier cooling flip, with longer Auger recombination times in hybrid perovskite nanocrystals resulting in longer persistent hot carriers. Upon the basis of these experiments, as well as a growing body of literature identifying a“hot phonon bottleneck” which occurs only above threshold excitation densities in bulk or nanocrystalline perovskites, neither all-inorganic nor hybrid organic-inorganic perovskite nanocrystals displays dramatically more amenable physics for hot carrier photovoltaics than bulk gallium arsenide, which in most respects they closely resemble.

6. Experimental Section

Materials. Lead bromide (98 %), cesium carbonate (99 %), formamidinium (FA) acetate (99 %), octadecene (90%), oleic acid (90%), and oleylamine (70%) were purchased from Sigma-Aldrich. All solvents were ACS grade or higher.

Synthesis. Synthesis of $CsPbBr_3$ and $FAPbBr_3$ nanocrystals (NCs) followed literature procedures of hot injection.[21,22] To prepare $FAPbBr_3$ NCs, an injection solution of 521 mg formamidinium acetate dissolved in 20 mL of oleic acid was dried under vacuum at 130 °C for 1 hour then stored at 50 °C for injections. For $CsPbBr_3$, an injection solution of 407 mg cesium carbonate was heated in 1.25 mL of oleic acid and 20 mL octadecene to 120 °C and held 1 hour to dry, then cooled to 100 °C for injections. Reactions were performed with 69 mg lead bromide dissolved at 120 °C under vacuum in a mixture of 5 mL octadecene, 0.5 mL oleylamine, and 0.5 mL oleic acid. Subsequently the reaction temperatures were adjusted to between 115 °C to 200 °C depending on the composition and desired relative size. As-synthesized samples were highly fluorescent consistent with earlier quantum yield reports of >50 %.[21,22] Carrier cooling dynamics were therefore not believe to be dominated by trapping.

Microscopy. Transmission electron microscopy (TEM) was performed using a JEOL 2100f instrument with sizing analysis done in ImageJ.

X-ray Diffraction. X-ray diffraction data for the representative samples was collected using a Cu k-α source with a Bruker D2 phaser instrument with samples prepared by drop-casting on to a miscut silicon wafer.

Optical absorption. UV-visible absorption measurements were performed on liquid samples in toluene using a Cary 50 spectrometer in 1 mm cuvettes.

Transient Absorption (TA) Spectroscopy. Except for low-temperature measurements, TA measurements were performed on 1-mm pathlength cuvettes with particle dispersions in toluene. For low-temperature measurements, drop-cast solid nanocrystal films were prepared on a sapphire disk. Below room temperature, the sample spots show greatly-increased scattering of the pump beam, attributed to crystallization of excess organic ligand. TA measurements were performed with a white light probe generated using the focused 1.55 eV output of a Ti: sapphire

amplifier through a sapphire or CaF_2 plate. Pump excitations beams were made by frequency-doubling a fraction of the amplifier output (for 3.1 eV) or using an optical parametric amplifier to generate other pump photon energies. Time-resolution of the experiments was approximately 60 fs and spectral resolution approximately 13 nm as configured. Excitonic absorption rise times were extracted from the experimental data by fitting with an exponential decay of the form $\Delta\alpha = ae^{t/\tau} + b$, where a and b are scalars. Boltzmann distributions were estimated following literature examples by fitting the blue side of the excitonic bleach to a function of the form $\Delta\alpha = ae^{\left(-\frac{E}{kT}\right)} + b$ where *k* is Boltzmann's constant, *E* is photon energy, *a* is a scalar, and *b* is an offset reflecting photoinduced absorption.[12,34,35]

Ultrafast Photoluminescence Spectroscopy. Time-resolved photoluminescence was collected using a single-photon-sensitive streak camera synchronized with a 3.1 eV pump excitation beam made by frequency-doubling the output of a Ti: sapphire amplifier. Pulsewidth is approximately 30 fs; instrument response for the time-resolved photoluminescence experiments was approximately 10 ps as configured.

Supporting Information

Supporting Information is available from the Wiley Online Library or from the author.

Acknowledgements

This work was performed at the Center for Nanoscale Materials, a U.S. Department of Energy Office of Science User Facility, and supported by the U.S. Department of Energy, Office of Science, under Contract No. DE-AC02-06CH11357.

Received: ((will be filled in by the editorial staff))
Revised: ((will be filled in by the editorial staff))
Published online: ((will be filled in by the editorial staff))

References

[1] G. E. Eperon, S. D. Stranks, C. Menelaou, M. B. Johnston, L. M. Herz, H. J. Snaith, *Energy Environ. Sci.* **2014**, *7*, 982.

[2] S. D. Stranks, G. E. Eperon, G. Grancini, C. Menelaou, M. J. P. Alcocer, T. Leijtens, L. M. Herz, A. Petrozza, H. J. Snaith, *Science* **2013**, *342*, 341.

[3] A. Poglitsch, D. Weber, *J. Chem. Phys.* **1987**, *87*, 6373.

[4] M. A. Pérez-Osorio, R. L. Milot, M. R. Filip, J. B. Patel, L. M. Herz, M. B. Johnston, F. Giustino, *J. Phys. Chem. C* **2015**, *119*, 25703.

[5] J. Even, L. Pedesseau, C. Katan, *J. Phys. Chem. C* **2014**, *118*, 11566.

[6] V. D'Innocenzo, G. Grancini, M. J. P. Alcocer, A. R. S. Kandada, S. D. Stranks, M. M. Lee, G. Lanzani, H. J. Snaith, A. Petrozza, *Nat. Commun.* **2014**, *5*, 3586.

[7] L. Q. Phuong, Y. Yamada, M. Nagai, N. Maruyama, A. Wakamiya, Y. Kanemitsu, *J. Phys. Chem. Lett.* **2016**, *7*, 2316.

[8] T. Etienne, E. Mosconi, F. De Angelis, *J. Phys. Chem. Lett.* **2016**, *7*, 1638.

[9] C. Quarti, E. Mosconi, F. De Angelis, *Phys. Chem. Chem. Phys.* **2015**, *17*, 9394.

[10] G. E. Eperon, E. Jedlicka, D. S. Ginger, *J. Phys. Chem. Lett.* **2018**, *9*, 104.

[11] M. E. Madjet, G. R. Berdiyorov, F. El-Mellouhi, F. H. Alharbi, A. V. Akimov, S. Kais, *J. Phys. Chem. Lett.* **2017**, *8*, 4439.

[12] H. Zhu, K. Miyata, Y. Fu, J. Wang, P. P. Joshi, D. Niesner, K. W. Williams, S. Jin, X.-Y. Zhu, *Science* **2016**, *353*, 1409.

[13] D. Niesner, H. Zhu, K. Miyata, P. P. Joshi, T. J. S. Evans, B. J. Kudisch, M. T. Trinh, M. Marks, X.-Y. Zhu, *J. Am. Chem. Soc.* **2016**, *138*, 15717.

[14] R. T. Ross, A. J. Nozik, *J. Appl. Phys.* **1982**, *53*, 3813.

[15] Y. Takeda, T. Ito, T. Motohiro, D. König, S. Shrestha, G. Conibeer, *J. Appl. Phys.* **2009**, *105*, 074905.

[16] P. Papagiorgis, L. Protesescu, M. V. Kovalenko, A. Othonos, G. Itskos, *J. Phys. Chem. C* **2017**, *121*, 12434.

[17] Q. Shen, T. S. Ripolles, J. Even, Y. Ogomi, K. Nishinaka, T. Izuishi, N. Nakazawa, Y. Zhang, C. Ding, F. Liu, T. Toyoda, K. Yoshino, T. Minemoto, K. Katayama, S. Hayase, *Appl. Phys. Lett.* **2017**, *111*, 153903.

[18] H.-H. Fang, S. Adjokatse, S. Shao, J. Even, M. A. Loi, *Nat. Commun.* **2018**, *9*, 243.

[19] H. Kawai, G. Giorgi, A. Marini, K. Yamashita, *Nano Lett.* **2015**, *15*, 3103.

[20] T. R. Hopper, A. Gorodetsky, J. M. Frost, C. Müller, R. Lovrincic, A. a. Bakulin, *ACS Energy Lett.* **2018**, 2199.

[21] L. Protesescu, S. Yakunin, M. I. Bodnarchuk, F. Krieg, R. Caputo, C. H. Hendon, R. X. Yang, A. Walsh, M. V. Kovalenko, *Nano Lett.* **2015**, *15*, 3692.

[22] L. Protesescu, S. Yakunin, M. I. Bodnarchuk, F. Bertolotti, N. Masciocchi, A. Guagliardi, M. V. Kovalenko, *J. Am. Chem. Soc.* **2016**, *138*, 14202.

[23] A. J. Nozik, C. A. Parsons, D. J. Dunlavy, B. M. Keyes, R. K. Ahrenkiel, *Solid State Commun.* **1990**, *75*, 297.

[24] W. Pötz, *Phys. Rev. B* **1987**, *36*, 5016.

[25] Y. Rosenwaks, M. C. Hanna, D. H. Levi, D. M. Szmyd, R. K. Ahrenkiel, A. J. Nozik, *Phys. Rev. B* **1993**, *48*, 14675.

[26] R. F. Leheny, J. Shah, R. L. Fork, C. V. Shank, a. Migus, *Solid State Commun.* **1979**, *31*, 809.

[27] E. J. Yoffa, *Phys. Rev. B* **1981**, *23*, 1909.

[28] M. C. Downer, C. V. Shank, *Phys. Rev. Lett.* **1986**, *56*, 761.

[29] M. Achermann, A. P. Bartko, J. A. Hollingsworth, V. I. Klimov, *Nat. Phys.* **2006**, *2*, 557.

[30] E. Baghani, S. K. Oleary, I. Fedin, D. V. Talapin, M. Pelton, *J. Phys. Chem. Lett.* **2015**, *6*, 1032.

[31] M. Pelton, S. Ithurria, R. D. Schaller, D. S. Dolzhnikov, D. V. Talapin, *Nano Lett.* **2012**, *12*, 6158.

[32] P. Cottingham, R. L. Brutchey, *Chem. Commun.* **2016**, *52*, 5246.

[33] J. M. Richter, F. Branchi, F. V. de A. Camargo, B. Zhao, R. H. Friend, G. Cerullo, F. Deschler, *Nat. Commun.* **2017**, 1.

[34] Y. Yang, D. P. Ostrowski, R. M. France, K. Zhu, J. van de Lagemaat, J. M. Luther, M. C. Beard, *Nat. Photonics* **2015**, *10*, 53.

[35] A. Mondal, J. Aneesh, V. Kumar Ravi, R. Sharma, W. J. Mir, M. C. Beard, A. Nag, K. V. Adarsh, *Phys. Rev. B* **2018**, *98*, 115418.

[36] V. I. Klimov, *Annu. Rev. Phys. Chem.* **2007**, *58*, 635.

[37] H. Benisty, *Phys. Rev. B* **1995**, *51*, 13281.

[38] H. Benisty, C. M. Sotomayor-Torrès, C. Weisbuch, *Phys. Rev. B* **1991**, *44*, 10945.

[39] U. Bockelmann, G. Bastard, *Phys. Rev. B* **1990**, *42*, 8947.

[40] I. Levchuk, A. Osvet, X. Tang, M. Brandl, J. D. Perea, F. Hoegl, G. J. Matt, R. Hock, M. Batentschuk, C. J. Brabec, *Nano Lett.* **2017**, *17*, 2765.

[41] A. L. Efros, V. A. Kharchenko, M. Rosen, *Solid State Commun.* **1995**, *93*, 281.

[42] J. Harbold, H. Du, T. Krauss, K.-S. Cho, C. B. Murray, F. Wise, *Phys. Rev. B* **2005**, *72*, 1.

[43] V. I. Klimov, D. W. McBranch, C. A. Leatherdale, M. G. Bawendi, *Phys. Rev. B* **1999**, *60*, 13740.

[44] M. Li, S. Bhaumik, T. W. Goh, M. S. Kumar, N. Yantara, M. Grätzel, S. Mhaisalkar, N. Mathews, T. C. Sum, *Nat. Commun.* **2017**, *8*, 14350.

[45] D. Bozyigit, N. Yazdani, M. Yarema, O. Yarema, W. M. M. Lin, S. Volk, K. Vuttivorakulchai, M. Luisier, F. Juranyi, V. Wood, *Nature* **2016**, *531*, 618.

[46] R. E. Brandt, V. Stevanović, D. S. Ginley, T. Buonassisi, *MRS Commun.* **2015**, *5*, 1.

[47] P. Guyot-Sionnest, B. Wehrenberg, D. Yu, *J. Chem. Phys.* **2005**, *123*, 074709.

[48] A. Aharoni, D. Oron, U. Banin, E. Rabani, J. Jortner, *Phys. Rev. Lett.* **2008**, *100*, 1.

[49] R. E. Brandt, J. R. Poindexter, P. Gorai, R. C. Kurchin, R. L. Z. Hoye, L. Nienhaus, M. W. B. Wilson, J. A. Polizzotti, R. Sereika, R. Žaltauskas, L. C. Lee, J. L. MacManus-Driscoll, M. Bawendi, V. Stevanović, T. Buonassisi, *Chem. Mater.* **2017**, *29*, 4667.

[50] N. Yazdani, T. Nguyen-Thanh, M. Yarema, W. M. M. Lin, R. Gao, O. Yarema, A. Bosak, V. Wood, *J. Phys. Chem. Lett.* **2018**, *9*, 1561.

[51] R. D. Schaller, J. M. Pietryga, S. V. Goupalov, M. A. Petruska, S. A. Ivanov, V. I. Klimov, *Phys. Rev. Lett.* **2005**, *95*, 1.

[52] J. Fu, Q. Xu, G. Han, B. Wu, C. H. A. Huan, M. L. Leek, T. C. Sum, *Nat. Commun.* **2017**, *8*, 1300.

[53] W. Lee, H. Li, A. B. Wong, D. Zhang, M. Lai, Y. Yu, Q. Kong, E. Lin, J. J. Urban, J. C. Grossman, P. Yang, *Proc. Natl. Acad. Sci.* **2017**, *114*, 201711744.

[54] C. K. MØLLER, *Nature* **1958**, *182*, 1436.

[55] B. T. Diroll, H. Zhou, R. D. Schaller, *Adv. Funct. Mater.* **2018**, *28*, 1800945.

[56] B. T. Diroll, G. Nedelcu, M. V. Kovalenko, R. D. Schaller, *Adv. Funct. Mater.* **2017**, *3*, 1606750.

[57] B. T. Diroll, P. Guo, R. D. Schaller, *Nano Lett.* **2018**, *18*, 846.

[58] X. Li, Y. Wu, S. Zhang, B. Cai, Y. Gu, J. Song, H. Zeng, *Adv. Funct. Mater.* **2016**, *26*, 2435.

[59] H.-H. Fang, L. Protesescu, D. M. Balazs, S. Adjokatse, M. V. Kovalenko, M. A. Loi, *Small* **2017**, *13*, 1700673.

[60] G. J. Hedley, C. Quarti, J. Harwell, O. V. Prezhdo, D. Beljonne, I. D. W. Samuel, *Sci. Rep.* **2018**, *8*, 1.

[61] P. Borri, S. Ceccherini, M. Gurioli, F. Bogani, *Solid State Commun.* **1997**, *103*, 77.

[62] Q. Liu, Y. Wang, N. Sui, Y. Wang, X. Chi, Q. Wang, Y. Chen, W. Ji, L. Zou, H. Zhang, *Sci. Rep.* **2016**, *6*, 29442.

[63] J. Yang, X. Wen, H. Xia, R. Sheng, Q. Ma, J. Kim, P. Tapping, T. Harada, T. W. Kee, F. Huang, Y.-B. Cheng, M. Green, A. Ho-Baillie, S. Huang, S. Shrestha, R. Patterson, G. Conibeer, *Nat. Commun.* **2017**, *8*, 14120.

[64] V. I. Klimov, *Science* **2000**, *287*, 1011.

[65] R. P. Joshi, D. K. Ferry, *Phys. Rev. B* **1989**, *39*, 1180.

[66] N. S. Makarov, S. Guo, O. Isaienko, W. Liu, I. Robel, V. I. Klimov, *Nano Lett.* **2016**, *16*, 2349.

[67] S. Yakunin, L. Protesescu, F. Krieg, M. I. Bodnarchuk, G. Nedelcu, M. Humer, G. De Luca, M. Fiebig, W. Heiss, M. V. Kovalenko, G. De Luca, M. Fiebig, W. Heiss, M. V. Kovalenko, *Nat. Commun.* **2015**, *6*, 8056.

[68] F. Garcia-Santamaria, Y. Chen, J. Vela, R. D. Schaller, J. A. Hollingsworth, V. I. Klimov, *Nano Lett.* **2009**, *9*, 3482.

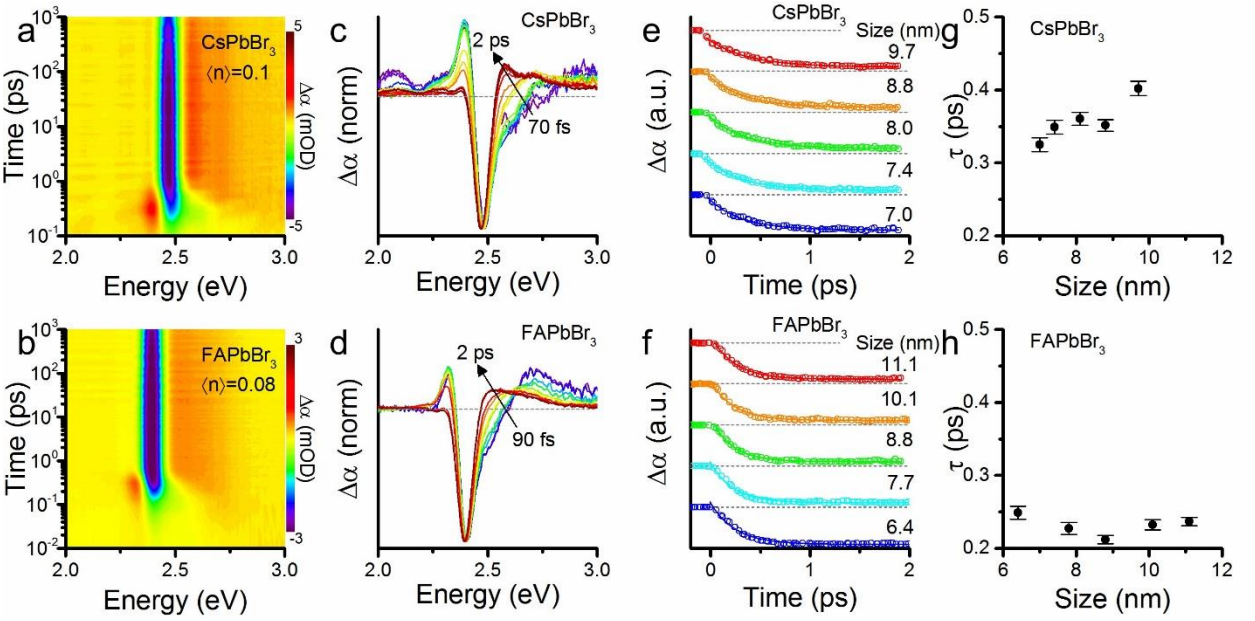

Figure 1. Time- and energy-resolved maps of transient absorption with 3.1 eV pump of representative (b) 9.7 nm $CsPbBr_3$ and (b) 8.8 nm $FAPbBr_3$ nanocrystals. (c, d) Normalized spectral line-cuts of the two-dimensional maps. (e, f) Kinetics of the excitonic bleach feature for a series of (e) $CsPbBr_3$ and (f) $FAPbBr_3$ nanocrystals of various sizes. Data presented as open circles with solid single fit lines. (g, h) Extracted fits from (e, f) plotted against nanocrystal size. Gray dashed lines in (c, d, e, f) indicate $\Delta\alpha = 0$ for each respective trace.

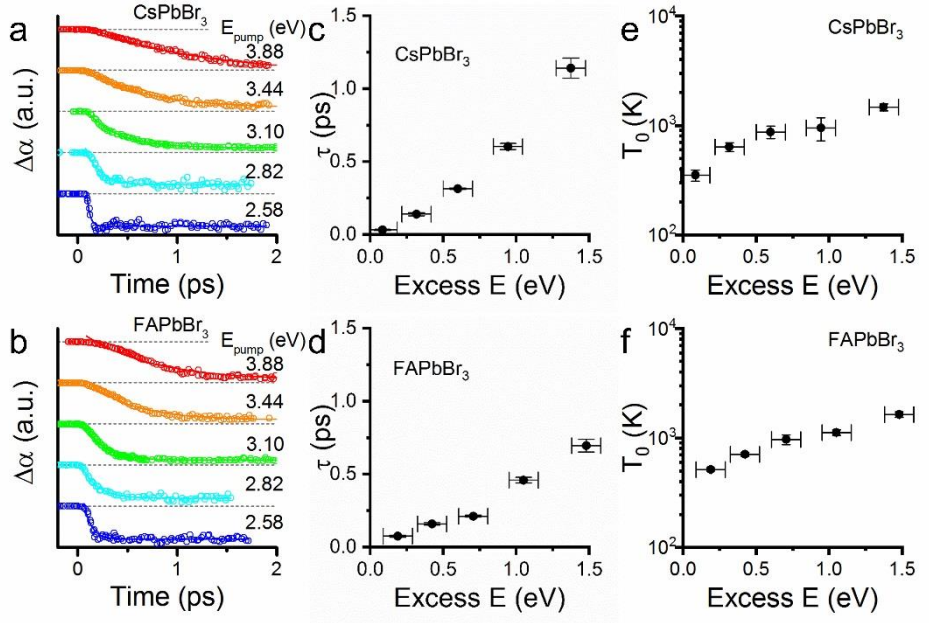

Figure 1. Transient absorption dynamics at the excitonic bleach of (a) 8.8 nm $CsPbBr_3$ and (b) 8.8 nm $FAPbBr_3$ nanocrystals at several pump excitation energies. The pump fluence was adjusted in each case to the single-exciton regime, calibrated in detail for 3.1 eV pump and adjusted thereafter using the bleach intensity. Data are shown in open circles with an exponential decay fitted as a solid line. (c, d) Intraband relaxation times from experimental fitting plotted against the excess energy of the pump beam. Energy in excess of the band gap

was estimated based upon the center energy of the excitonic bleach of the semiconductor nanocrystals. The band width of the femtosecond laser was used to estimate the error in the excess energy. (e, f) Initial carrier temperatures estimated for different excess energies based upon Boltzmann fitting of the blue tail of transient absorption bleaching just after thermalization (100-200 fs delay). Gray dashed lines in (a, b) indicate $\Delta\alpha = 0$ for each respective trace.

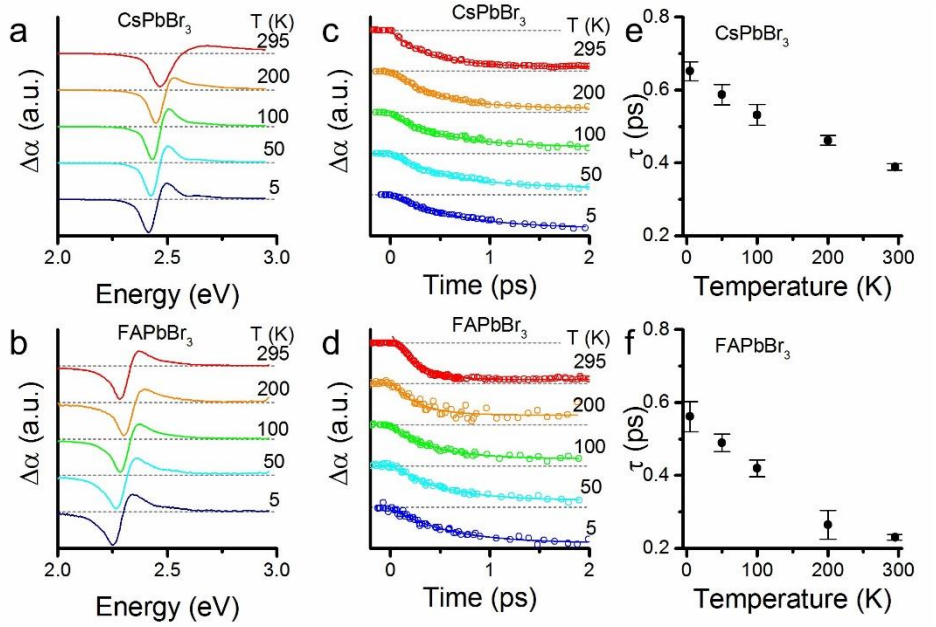

Figure 3. Low-fluence transient absorption spectra collected at ~3 ps delay times with 3.1 eV pump for (a) 9.7 nm $CsPbBr_3$ and (b) 8.8 nm $FAPbBr_3$ at the designated temperatures. (c, d) Temperature-dependent bleaching kinetics at the excitonic bleach feature of the same samples. Data in open circles and solid fit lines represent exponential fits to the data. (e, f) Scatterplots of the interband relaxation time fitted in (c, d) against temperature. Gray dashed lines in (a, b, c, d) indicate $\Delta\alpha = 0$ for each respective trace.

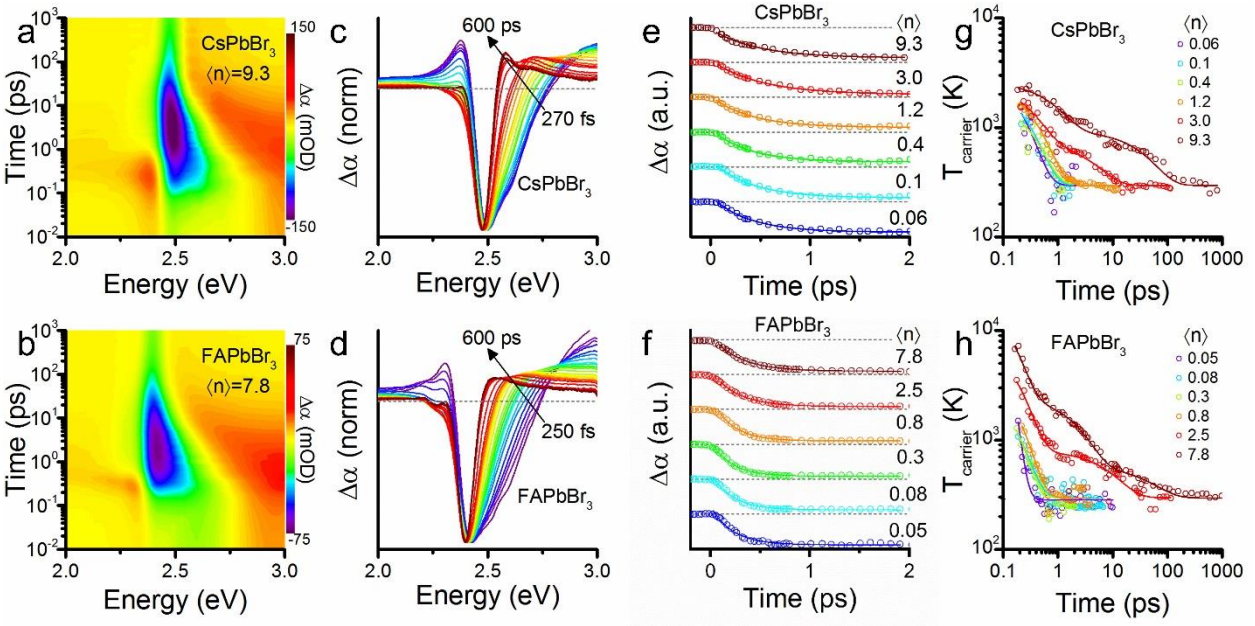

Figure4. Time- and energy-resolved contour plots of transient absorption data with 3.1 eV pump energy collected for (a) 9.7 nm $CsPbBr_3$ and (b) 8.8 nm $FAPbBr_3$ nanocrystals in the multiple electron-hole pairs *per* nanocrystal regime. (c, d) Spectral line-cuts from (a) and (b), respectively. (e, f) Transient absorption collected at several pump fluences at the excitonic bleach. (g, h) Time-dependence of carrier temperature at different fluences for $CsPbBr_3$ and $FAPbBr_3$ nanocrystals. Solid fit lines to the data in open circles represent monoexponential decays in the single electron-hole pair *per* nanocrystal regime and polyexponential decays in the multiple electron-hole pairs *per* nanocrystal regime. Fitting data are reported in Supporting Information Tables S2 and S3.

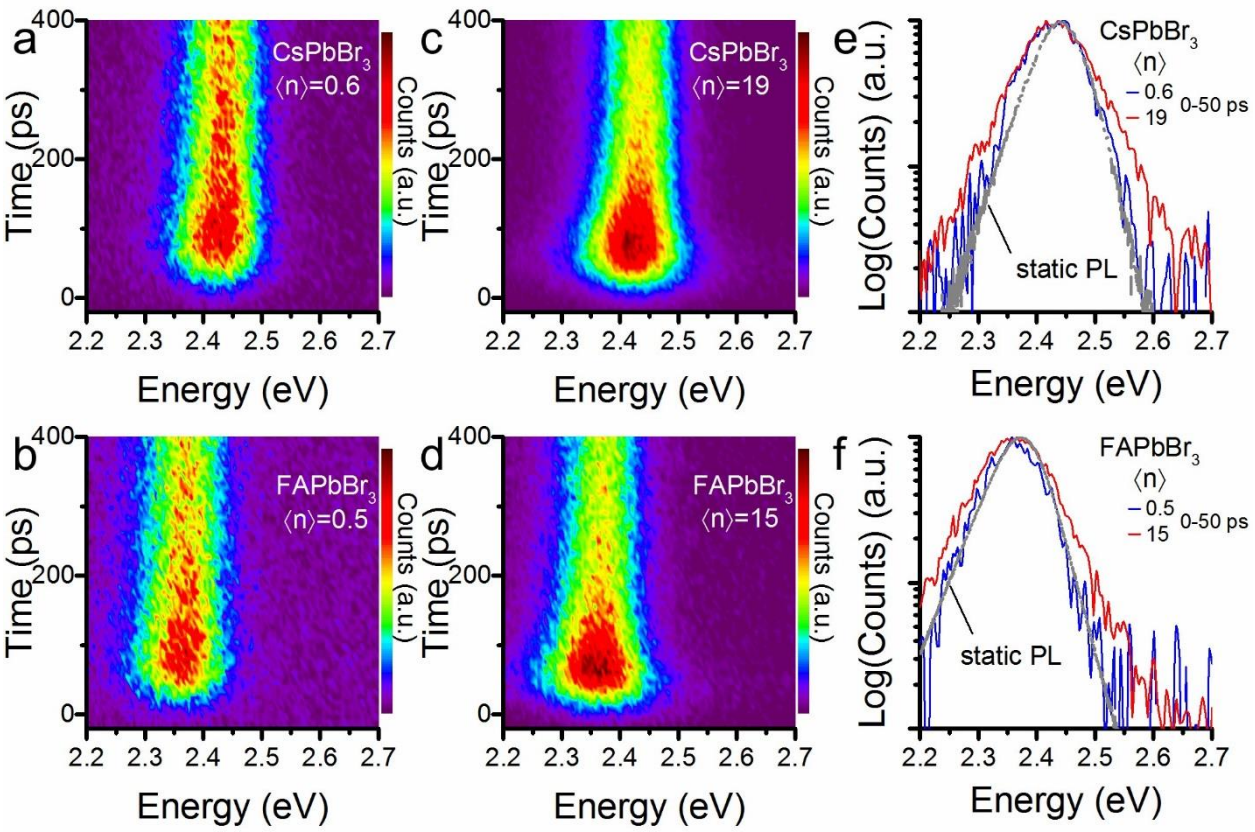

Figure 2. Time- and energy-resolved maps of photoluminescence of (a) 9.7 nm $CsPbBr_3$ and (b) 8.8 nm $FAPbBr_3$ nanocrystals at low fluence with 3.1 eV pump excitation. (c, d) Corresponding samples at high fluence (multiple electron hole pairs *per* nanocrystal) regime. (e, f) Comparison of the integrated photoluminescence for the first 50 ps of emission under high- and low-fluence conditions with the time-integrated emission under low-fluence excitation (gray lines).

Intraband cooling in all-inorganic $CsPbBr_3$ and hybrid organic-inorganic $FAPbBr_3$ nanocrystals reveal longer cooling times in $CsPbBr_3$ at low fluence. Persistent hot carriers beyond 2 picoseconds are not observed in either set of nanocrystals except in the multiple electron-hole pairs *per* nanocrystal regime.

Perovskites

*Benjamin T. Diroll and Richard D. Schaller**

Intraband Cooling in All-Inorganic and Hybrid Organic-Inorganic Perovskite Nanocrystals

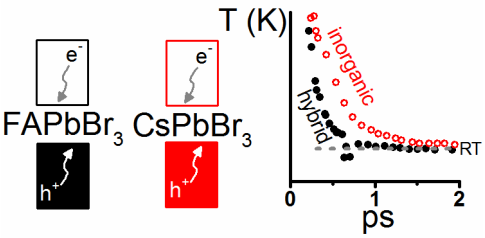

Supporting Information

Intraband Cooling in All-Inorganic and Hybrid Organic-Inorganic Perovskite Nanocrystals

*Benjamin T. Diroll and Richard D. Schaller**

Supporting Data

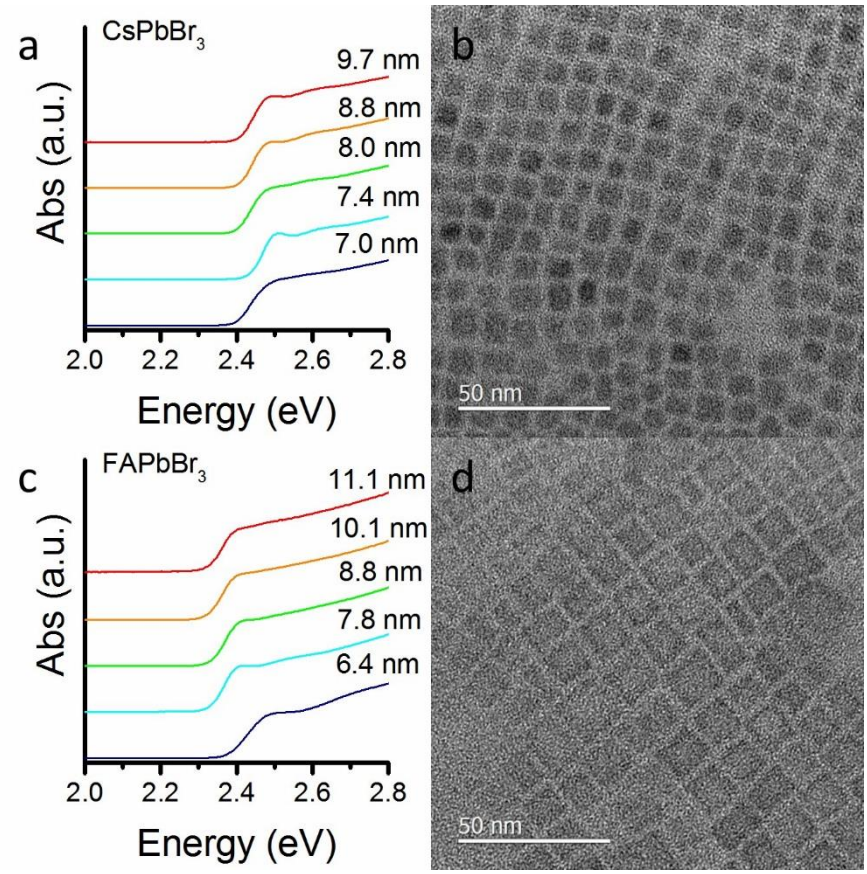

Figure S1. (a) Absorption of size-dependent series of $CsPbBr_3$ nanocrystals. (b) TEM image of 8.0 nm $CsPbBr_3$ NCs. (c) Absorption of size-dependent series of $FAPbBr_3$ NCs. (d) TEM image of 10.1 nm $FAPbBr_3$ nanocrystals.

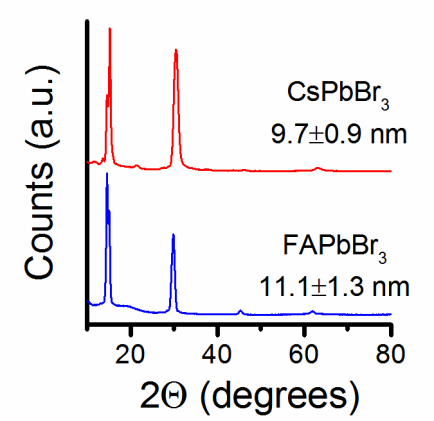

Figure S2. X-ray diffraction patterns of representative nanocrystal samples used in this work. The data match previous reports of orthorhombic $CsPbBr_3$ nanocrystals[32] and cubic $FAPbBr_3$ nanocrystals.[22]

Table S1. Size of Nanocrystals Used in Work

$CsPbBr_3$ Sample	Size (nm)	$FAPbBr_3$ Sample	Size (nm)
1	9.7±0.9	1	11.1±1.3
2	8.8±0.8	2	10.1±1.6
3	8.0±0.9	3	8.8±1.1
4	7.4±0.8	4	7.8±1.1
5	7.0±1.0	5	6.4±1.0

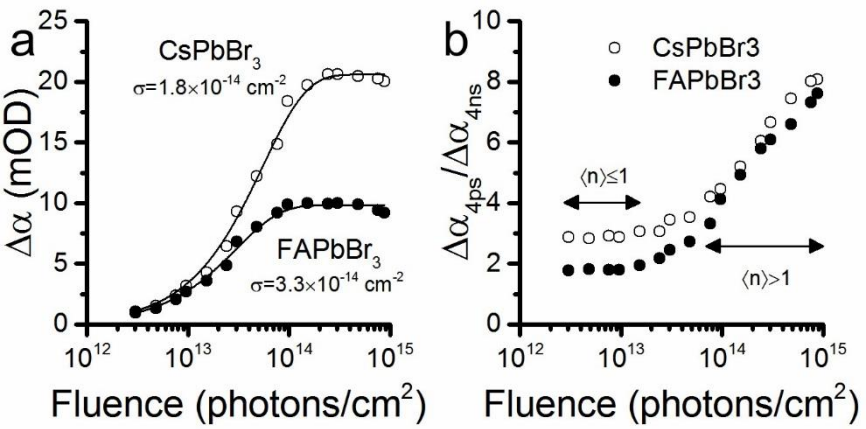

Figure S3. (a) Bleach intensity at 4 ps delay time as a function of fluence for 9.7 nm $CsPbBr_3$ and 8.8 nm $FAPbBr_3$. Solid exponential growth of the form $A(1-e^{-x\sigma})$ permit extraction of an absorption cross section.[68] The measurements were performed at 3.1 eV pump energy. Using the cross-section of a sample thus measured, the electron-hole pairs absorbed at a given fluence is calculated by multiplying the fluence by the cross-section.

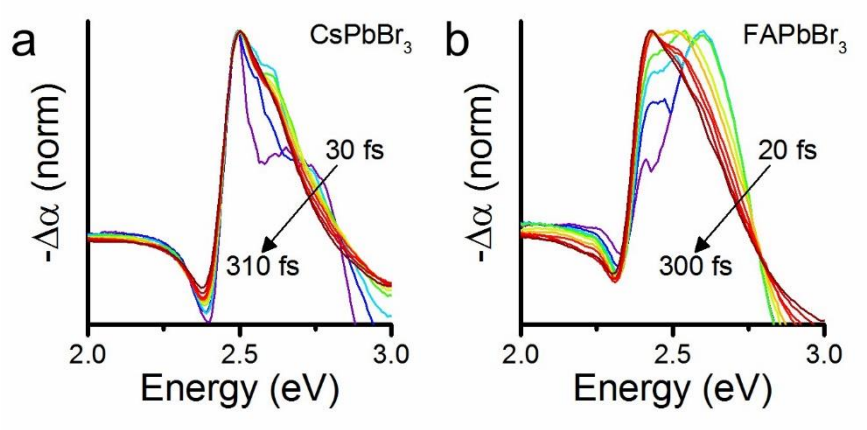

Figure S4. Early time transient normalized transient spectra of (a) 9.7 nm $CsPbBr_3$ and (b) 8.8 nm $FAPbBr_3$ nanocrystals at an average of 9.3 and 7.8 electron-hole pairs *per* nanocrystal, respectively.

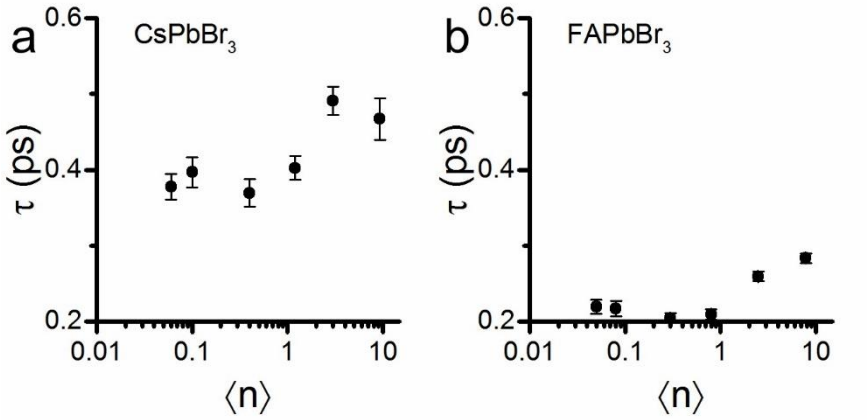

Figure S5. Fluence-dependent lifetime of the excitonic maximum rise in (a) 9.7 nm $CsPbBr_3$ and (b) 8.8 nm $FAPbBr_3$ nanocrystals.

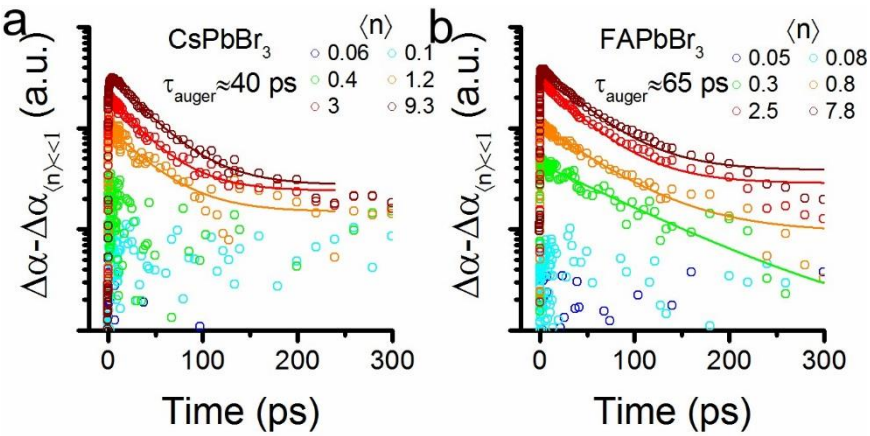

Figure S6. Fluence-dependent differenced TA data for (a) 9.7 nm $CsPbBr_3$ and (b) 8.8 nm $FAPbBr_3$ nanocrystals. Estimates of the Auger recombination time associated with two electron-hole pairs *per* nanocrystal are given on the plots. More systematic experiments to ascertain the difference in Auger recombination times can be found in the literature (See main text reference 10).

Table S1. Fit parameters of carrier cooling of 9.7 nm $CsPbBr_3$ NCs at various excitation fluences, indicated by the average number of electron-hole pairs *per* nanocrystal (⟨n⟩).

⟨n⟩	τ_1(ps)	τ_2 (ps)
0.06	0.19±0.08	--
0.1	0.26±0.05	--
0.4	0.32±0.10	--
1.2	0.38±0.01	--
3.0	0.33±0.05	4.78±0.98
9.3	0.59±0.10	43.8±7.8

Table S2. Parameters of single and exponential fits to carrier cooling of 9.7 nm $FAPbBr_3$ NCs at various excitation fluences, indicated by the average number of electron-hole pairs *per* nanocrystal (⟨n⟩).

⟨n⟩	τ_1 (ps)	τ_2 (ps)	τ_3 (ps)
0.05	0.04±0.01	N/A	N/A
0.08	0.14±0.01	N/A	N/A
0.3	0.12±0.01	N/A	N/A
0.8	0.15±0.00	N/A	N/A
2.5	0.15±0.01	10.1±2.3	N/A
7.8	0.12±0.01	2.5±0.2	53.3±29.2